IOPscience iopscience.iop.org

Home Search Collections Journals About Contact us My IOPscience

The structural and physical properties of $Ba_{1-x}Sr_xFe_2As_2$ ($0 \leq x \leq 1$) and $Ba_{1-x}Sr_xFe_{1.8}Co_{0.2}As_2$ ($0 \leq x \leq 1$)

This article has been downloaded from IOPscience. Please scroll down to see the full text article.

2009 J. Phys.: Condens. Matter 21 495701

(http://iopscience.iop.org/0953-8984/21/49/495701)

View the table of contents for this issue, or go to the journal homepage for more

Download details:
IP Address: 129.252.86.83
The article was downloaded on 30/05/2010 at 06:22

Please note that terms and conditions apply.

J. Phys.: Condens. Matter **21** (2009) 495701 (5pp) doi:10.1088/0953-8984/21/49/495701

The structural and physical properties of $Ba_{1-x}Sr_xFe_2As_2$ ($0 \leqslant x \leqslant 1$) and $Ba_{1-x}Sr_xFe_{1.8}Co_{0.2}As_2$ ($0 \leqslant x \leqslant 1$)

Zhiwei Wang, Huaixin Yang, Chao Ma, Huanfang Tian, Honglong Shi, Jiangbo Lu, Lunjie Zeng and Jianqi Li[1]

Beijing National Laboratory for Condensed Matter Physics, Institute of Physics, Chinese Academy of Sciences, Beijing 100190, People's Republic of China

E-mail: LJQ@aphy.iphy.ac.cn

Received 24 July 2009, in final form 14 October 2009
Published 12 November 2009
Online at stacks.iop.org/JPhysCM/21/495701

Abstract

Polycrystalline samples of $Ba_{1-x}Sr_xFe_2As_2$ ($0 \leqslant x \leqslant 1$) and $Ba_{1-x}Sr_xFe_{1.8}Co_{0.2}As_2$ ($0 \leqslant x \leqslant 1$) have been synthesized by a solid state reaction method. Structural analysis by means of x-ray diffraction shows that the lattice parameters and unit cell volume decrease monotonically with the increase of x for $Ba_{1-x}Sr_xFe_2As_2$. The measurements of transport properties demonstrate that the average size of the Ba(Sr)-site cations could evidently influence the spin density wave (SDW) behavior in $Ba_{1-x}Sr_xFe_2As_2$ and superconductivity in $Ba_{1-x}Sr_xFe_{1.8}Co_{0.2}As_2$ as well. The critical temperature for SDW (T_{SDW}) increases with the Sr substitution for Ba in $Ba_{1-x}Sr_xFe_2As_2$ and, on the other hand, the superconducting T_c decreases with the increase of Sr content in $Ba_{1-x}Sr_xFe_{1.8}Co_{0.2}As_2$. The inhomogeneous distributions of Ba/Sr ions and structural distortions in $Ba_{0.5}Sr_{0.5}Fe_2As_2$ have been investigated by transmission-electron microscopy (TEM) observations.

(Some figures in this article are in colour only in the electronic version)

1. Introduction

Since the first iron-based layered superconductor $La[O_{1-x}F_x]FeAs$ with $T_c = 26$ K was reported in February 2008 [1], tremendous effort has been devoted to researching this new high-temperature superconductor. Recently, a variety of materials with a ZrCuSiAs-type structure (the so-called '1111' system) has been synthesized by substitution of La by Ce, Pr, Nd, Sm, Gd, etc [2–10]. These superconducting materials exhibit superconducting transitions ranging from $T_c = 20$ to 55 K. Moreover, similar to cuprate superconductors, the $(FeAs)^-$ layer is considered as the conducting layer playing a critical role for the occurrence of superconductivity, while the $(RO)^+$ layer (R = La, Ce, Pr, etc) injects charge carriers into the former by chemical doping and also retains the structural integrity of the $(FeAs)^-$ layer. In addition, another oxygen-free pnictide superconductor based on the parent AFe_2As_2 (abbreviated as the '122' system, A = Ca, Sr, Ba, Eu) with a $ThCr_2Si_2$-type structure was synthesized [11–18]. Similar to oxy-pnictide, the parent compounds AFe_2As_2 are metallic and show a clear SDW instability. They become superconductors when the SDW is suppressed, either by chemical doping with holes or electrons, or by applied hydrostatic pressure [19, 20].

The parent phase of the Fe-based superconducting materials generally show remarkable SDW anomalies at temperatures between 120 and 220 K, as observed in the measurements of electrical resistivity and magnetic susceptibility [21, 22]. For instance, $BaFe_2As_2$, $SrFe_2As_2$ and $CaFe_2As_2$ single crystals show phase transitions at about 140 K, 205 K and 170 K, respectively. These anomalies are often in connection with structural phase transitions at low temperatures [23]. Hole or electron doping leads to the suppression of the SDW and the appearance of superconductivity [14–16, 24]. In the present paper, we report on the structural properties of $Ba_{1-x}Sr_xFe_2As_2$ ($0 \leqslant x \leqslant 1$) and the superconductivity of $Ba_{1-x}Sr_xFe_{1.8}Co_{0.2}As_2$ ($0 \leqslant x \leqslant 1$).

[1] Author to whom any correspondence should be addressed.

 © 2009 IOP Publishing Ltd Printed in the UK

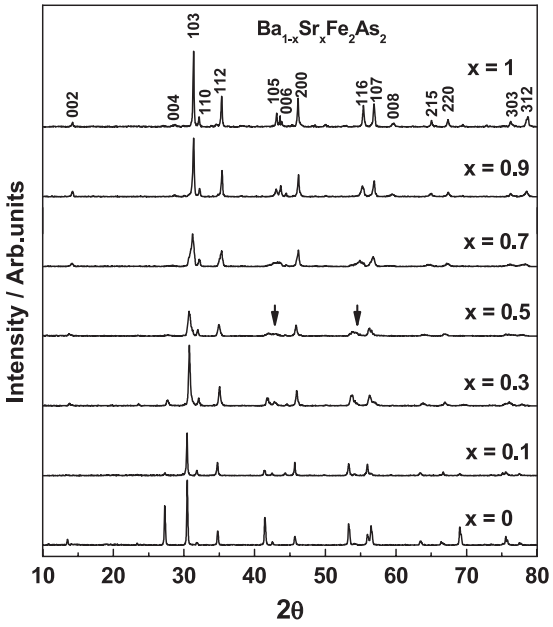

Figure 1. Powder x-ray diffraction pattern of $Ba_{1-x}Sr_xFe_2As_2$ ($x = 1$, 0.9, 0.7, 0.5, 0.3, 0.1 and 0).

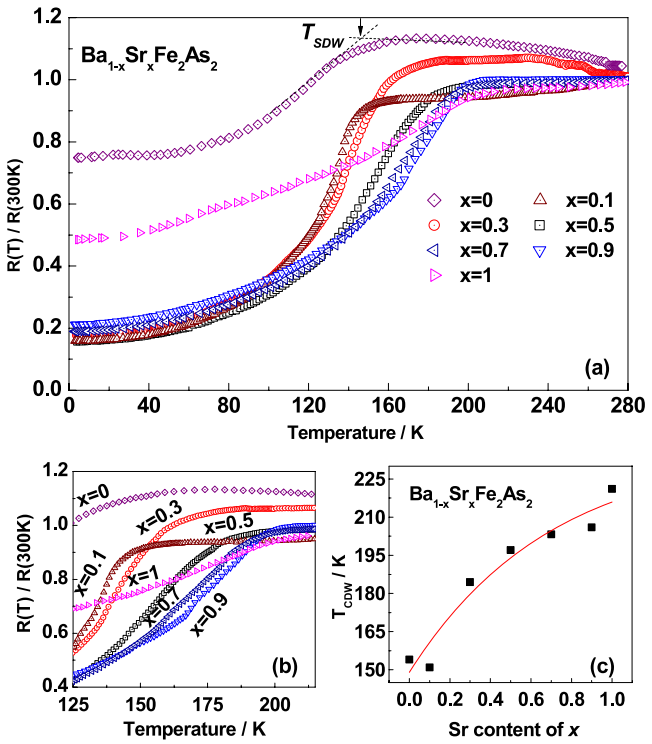

Figure 2. (a) Temperature dependence of the resistivity for the $Ba_{1-x}Sr_xFe_2As_2$ samples normalized to 300 K. The position of the SDW transition for $x = 0$ is indicated by an arrow (the crossing of the low tangents is shown in the picture). (b) An expanded view of the results for the resistivity near T_{SDW}, for clarity, showing the evolution of the SDW transition with Sr content. (c) The relationship of T_{SDW} as a function of x for the $Ba_{1-x}Sr_xFe_2As_2$ samples.

2. Experimental section

The polycrystalline samples of $Ba_{1-x}Sr_xFe_2As_2$ ($0 \leqslant x \leqslant 1$) were prepared by a conventional solid-state reaction method using $BaFe_2As_2$ and $SrFe_2As_2$ as starting materials. $BaFe_2As_2$ and $SrFe_2As_2$ were pre-synthesized by heating a Ba lump (99.99%) and an Sr lump (99.9%), Fe powder (99.9%) and an As piece (99.999%) in an evacuated quartz tube under 673 K, 873 K and 1073 K for 8 h, 12 h and 4 h, respectively. The raw materials were accurately weighed according to the stoichiometric ratio of $Ba_{1-x}Sr_xFe_2As_2$, and then the weighed powders were thoroughly ground and pressed into pellets. The pellets were sealed in an evacuated quartz tube and finally annealed at 1173 K for 24 h, then cooled to 973 K, where it was held for 12 h. Samples of $Ba_{1-x}Sr_xFe_{1.8}Co_{0.2}As_2$ ($0 \leqslant x \leqslant 1$) were also prepared in a similar method (described above) using $BaFe_2As_2$, $BaCo_2As_2$ and $SrFe_2As_2$ as starting materials. X-ray diffraction (XRD) measurements were carried out by an x-ray powder diffraction method with Cu Kα radiation at room temperature. The electrical resistivity as a function of temperature was measured by a standard four-point probe technique. Low-temperature magnetization measurements as a function of temperature were performed by using a commercial Quantum Design SQUID. Samples for TEM observations were prepared by the conventional method including cutting, mechanical polishing, dimpling and finalized by Ar^+ ion-beam thinning in the liquid nitrogen condition. Microstructural analyses were performed on a FEI Tecnai-F20 TEM operating at 200 kV.

3. Results and discussion

The crystal structures of the $Ba_{1-x}Sr_xFe_2As_2$ samples were first determined by x-ray powder diffraction. Figure 1 shows the results for $x = 1$, 0.9, 0.7, 0.5, 0.3, 0.1 and 0, in which all diffraction peaks could be well indexed to the tetragonal $ThCr_2Si_2$-type structure with a space group $I4/mmm$. The lattice parameters a, c and the unit cell volume are listed in table 1. It is recognizable that the lattice parameters and cell volume show a monotonic increase with the decrease of x, owing to the relatively larger size of Ba^{2+} cations in comparison with the Sr^{2+} cations. The lattice parameters of $BaFe_2As_2$ and $SrFe_2As_2$ obtained in our experiments are consistent with the data reported in earlier literature [13, 21]. It is also noted that the diffraction peak of the sample with $x = 0.5$ is visibly broader than others and some peaks split into two peaks as labeled by arrows in figure 1. This structural feature arises from the inhomogeneous distribution of Sr/Ba in this

Table 1. The lattice parameters a, c and the unit cell volume of $Ba_{1-x}Sr_xFe_2As_2$.

x	a (Å)	c (Å)	c/a	Unit cell volume (Å^3)
1.0	3.9205(±0.0003)	12.3275(±0.0010)	3.1444	189.4776
0.9	3.9254(±0.0013)	12.4498(±0.0065)	3.1716	191.8360
0.7	3.9485(±0.0022)	12.5282(±0.0053)	3.1729	195.3228
0.5	3.9542(±0.0007)	12.8274(±0.0036)	3.2440	200.5654
0.3	3.9565(±0.0008)	12.9133(±0.0058)	3.2638	202.1434
0.1	3.9702(±0.0016)	13.0376(±0.0082)	3.2839	205.5050
0	3.9784(±0.0032)	13.1096(±0.0087)	3.2952	207.4944

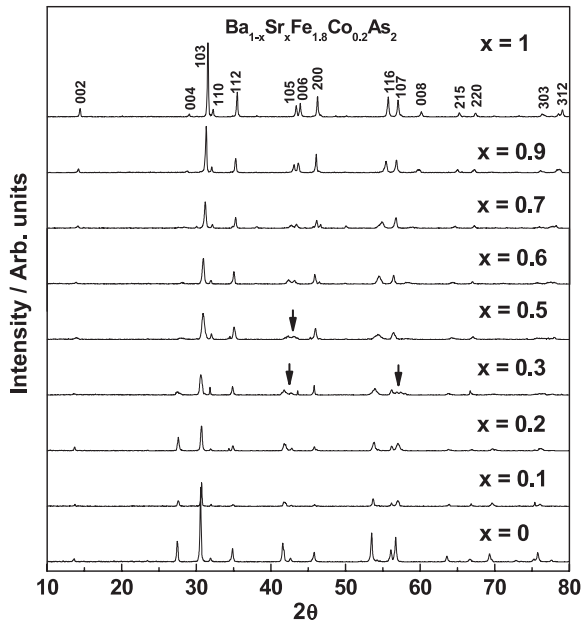

Figure 3. Powder x-ray diffraction pattern of $Ba_{1-x}Sr_xFe_{1.8}Co_{0.2}As_2$ ($x = 1$, 0.9, 0.7, 0.6, 0.5, 0.3, 0.2, 0.1 and 0).

Table 2. Lattice parameters a, c and the unit cell volume of $Ba_{1-x}Sr_xFe_{1.8}Co_{0.2}As_2$.

x	a (Å)	c (Å)	c/a	Unit cell volume (Å^3)
1.0	3.9245(±0.0005)	12.2884(±0.0020)	3.1312	189.2623
0.9	3.9253(±0.0012)	12.3464(±0.0057)	3.1453	190.2331
0.7	3.9342(±0.0036)	12.5822(±0.0057)	3.1982	194.7464
0.6	3.9482(±0.0041)	12.7129(±0.0019)	3.2199	198.1723
0.5	3.9516(±0.0047)	12.8376(±0.0027)	3.2487	200.4563
0.3	3.9459(±0.0037)	12.9314(±0.0085)	3.2771	201.3435
0.2	3.9498(±0.0032)	12.9283(±0.0093)	3.2732	201.6934
0.1	3.9547(±0.0011)	12.9138(±0.0039)	3.2655	201.9673
0	3.9611(±0.0016)	12.9623(±0.0048)	3.2724	203.3823

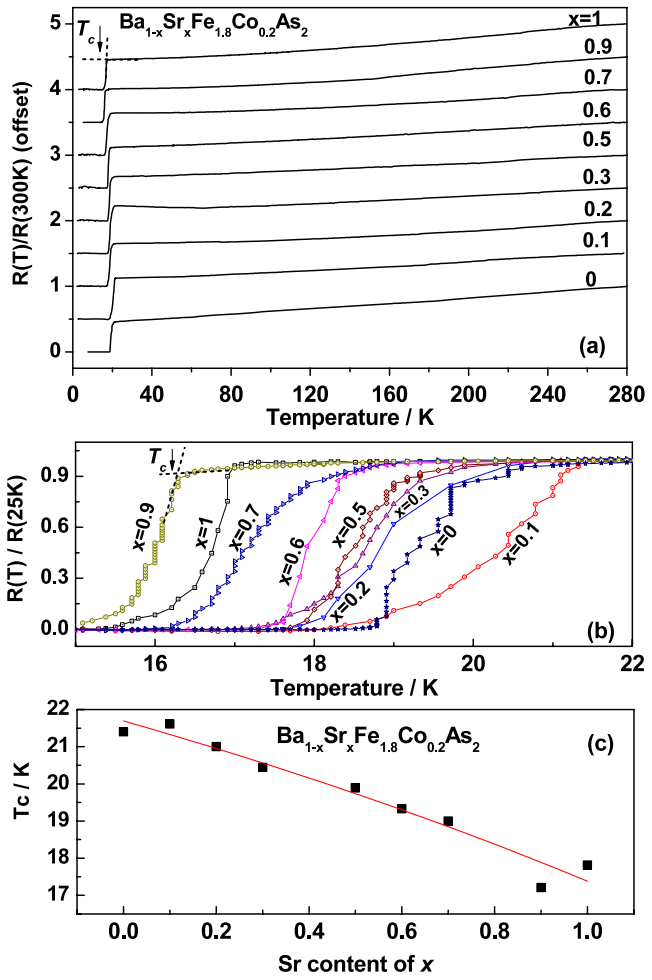

Figure 4. (a) Temperature dependence of the resistivity for the $Ba_{1-x}Sr_xFe_{1.8}Co_{0.2}As_2$ samples normalized to the data at 300 K and offset for clarity (all data are successfully offset vertically by 0.5 except for $x = 0$). (b) An expanded low-temperature view of the resistivity normalized to 25 K. The short arrows in (a) and (b) show the position of onset superconductivity transitions for the samples of $x = 1$ and 0.9, respectively. (c) The relationship of T_c as a function of x for the $Ba_{1-x}Sr_xFe_{1.8}Co_{0.2}As_2$ samples.

sample, which could result in clear local structural distortion as revealed by TEM investigations. Detailed microstructural analysis will be discussed in the following text.

It is well known that the $SrFe_2As_2$ and $BaFe_2As_2$ compounds show remarkable tetragonal to orthorhombic phase transitions in association with a spin density wave instability at temperatures of about 210 K and 140 K, respectively [21, 25]. Resistivity measurements of the $Ba_{1-x}Sr_xFe_2As_2$ samples show that the Sr content can evidently influence this phase transition and allows the critical temperature (T_{SDW}) to change towards low temperatures. Figure 2(a) shows the temperature dependence of the electrical resistivity of $Ba_{1-x}Sr_xFe_2As_2$. Clear SDW transitions can obviously be seen for all samples from an expanded low-temperature view near T_{SDW} as presented in figure 2(b). Figure 2(c) shows the changes of T_{SDW} with Sr content x and it is recognizable that the T_{SDW} in $Ba_{1-x}Sr_xFe_2As_2$ increases continuously with the increase of x.

It is also noted that the partial substitution of Co for Fe could introduce superconductivity in the AFe_2As_2 (A = Ba, Sr, Ca) system. We therefore synthesize a series of $Ba_{1-x}Sr_xFe_{1.8}Co_{0.2}As_2$ ($x = 0$, 0.1, 0.2, 0.3, 0.5, 0.6, 0.7, 0.9 and 1) samples to investigate the influence of the Sr content on the superconductivity. XRD patterns of these samples are shown in figure 3. It is clear that diffraction peaks of all polycrystalline samples could be well indexed to the $ThCr_2Si_2$-type structure. No clear diffraction peaks from impurities are observed in these x-ray diffraction data. The structural parameters for all samples are listed in table 2, illustrating the continuous changes of the lattice parameters a, c and the unit cell volume. It is recognizable that the cell volume increased progressively with the decrease of Sr content. On the other hand, dissimilar to the samples of $Ba_{1-x}Sr_xFe_2As_2$, lattice parameters and the c/a ratio show certain anomalous changes between $x = 0.1$ and 0.5. Moreover, careful analysis suggests that the diffraction peaks of the samples with $x = 0.5$ and 0.3 are visibly broadening, as indicated by the arrows in figure 3.

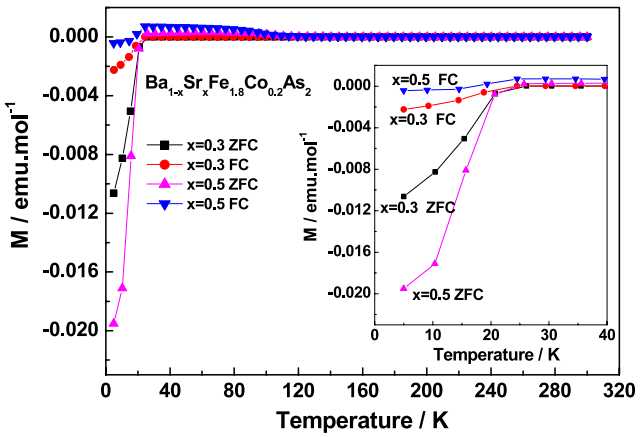

Figure 5. Temperature dependence of the magnetic susceptibility for the $Ba_{1-x}Sr_xFe_{1.8}Co_{0.2}As_2$ ($x = 0.3$ and 0.5) samples with a magnetic field of 10 Oe. The inset shows the magnetic susceptibility of low temperature near T_c.

Figure 4(a) shows the temperature dependence of electrical resistivity of the $Ba_{1-x}Sr_xFe_{1.8}Co_{0.2}As_2$ samples, exhibiting the presence of superconducting transitions for all samples with T_c ranging from 17.3 to 21.7 K. The onset temperature of the downturn in resistivity (the kink) was chosen as T_c, as labeled by the arrows. Figure 4(b) presents an expanded low-temperature view of the resistivity normalized to 25 K. Although the complex variation of resistivity often appears just above the superconductive critical temperature T_c, the T_c shows a notable decrease with the increase in Sr content, as shown in figure 4(c). The change tendency of T_c shows an opposite behavior with T_{SDW} as described in the above text. In our results, the highest T_c is observed in $Ba_{0.9}Sr_{0.1}Fe_{1.8}Co_{0.2}As_2$ at about 21.7 K.

Figure 5 shows the temperature dependence of zero-field-cooled (ZFC) and field-cooled (FC) magnetic susceptibility for two superconducting samples of $Ba_{0.5}Sr_{0.5}Fe_{1.8}Co_{0.2}As_2$ and $Ba_{0.7}Sr_{0.3}Fe_{1.8}Co_{0.2}As_2$ measured with an applied external magnetic field of 10 Oe. In both samples, the SDW anomalies that are clearly visible in $Ba_{0.5}Sr_{0.5}Fe_2As_2$ and $Ba_{0.7}Sr_{0.3}Fe_2As_2$ are notably suppressed. The onset diamagnetic transition starts at around 20 K, which is consistent with the results obtained from the measurements of resistivity as shown in figure 4(a).

In order to better understand the microstructure of these layered materials, we have performed an extensive x-ray and TEM analysis on $Ba_{1-x}Sr_xFe_2As_2$ and $Ba_{1-x}Sr_xFe_{1.8}Co_{0.2}As_2$. TEM observations indicate that the sample with a nominal composition of $Ba_{0.5}Sr_{0.5}Fe_2As_2$, often showing relatively broad reflection peaks (see figure 1), exhibits apparently inhomogeneous microstructure and complex structural distortions.

Figure 6(a) shows a selected-area electron diffraction pattern taken along the [100] zone axis direction. All main diffraction spots shown in these patterns can be well indexed by a tetragonal cell with lattice parameters of $a = 3.95$ Å and $c = 12.82$ Å, consistent with the x-ray diffraction data. Due to the presence of structural inhomogeneity and visible structural defects, the weak diffuse streaking of the high-order reflection spots can be clearly recognized in the diffraction pattern of figure 1.

A better and clear view of the structural layers of this sample has been obtained by high-resolution TEM investigations. Figure 6(b) shows a high-resolution electron micrograph of a $Ba_{0.5}Sr_{0.5}Fe_2As_2$ crystal taken along the [100] zone axis direction. These images were obtained from a region with clear structural distortion. These structural defects are considered as arising essentially from the inhomogeneous distributions of Ba/Sr ions in the crystal lattice. Moreover, we also performed the filtered TEM observations for directly mapping the Ba element in the $Ba_{0.5}Sr_{0.5}Fe_2As_2$ sample. Figure 6(c) shows a filtered TEM mapping illustrating the distribution of Ba in a $Ba_{0.5}Sr_{0.5}Fe_2As_2$ crystal. The visible alternation of the heavy and light contrast indicated the local inhomogeneity of Ba elements. This kind of structural defect could yield clear structural distortion and further a relatively wider superconducting transition in the $Ba_{0.5}Sr_{0.5}Fe_{1.8}Co_{0.2}As_2$ material.

4. Conclusions

We have successfully synthesized polycrystalline samples of $Ba_{1-x}Sr_xFe_2As_2$ ($0 \leqslant x \leqslant 1$) and $Ba_{1-x}Sr_xFe_{1.8}Co_{0.2}As_2$

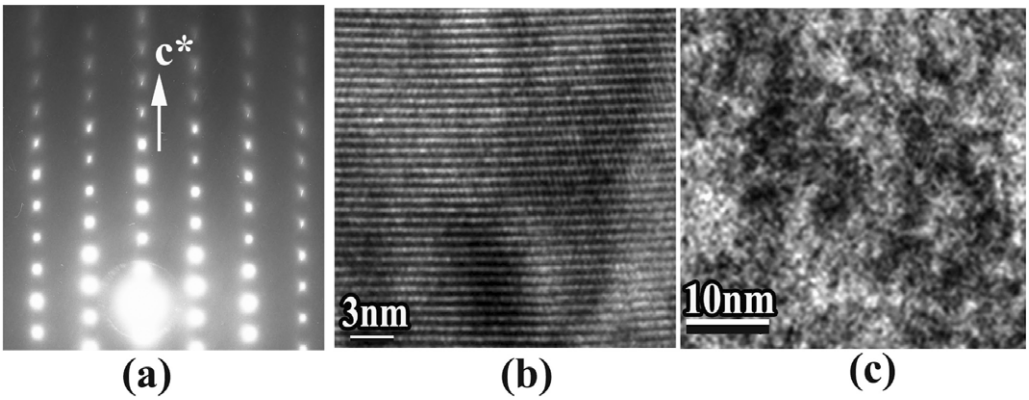

Figure 6. (a) Selected-area electron diffraction pattern $Ba_{0.5}Sr_{0.5}Fe_2As_2$ taken along the [100] zone axis direction. (b) High-resolution TEM images of a $Ba_{0.5}Sr_{0.5}Fe_2As_2$ crystal exhibiting distortion of structural layers. (c) Element mapping for Ba in a thin area showing the presence of clear contrast inhomogeneity.

($0 \leqslant x \leqslant 1$) by a solid-state reaction method. The structural properties and phase transition in correlation with SDW instability in $Ba_{1-x}Sr_xFe_2As_2$ have been characterized by the measurements of XRD and transport properties. Superconductivity in $Ba_{1-x}Sr_xFe_{1.8}Co_{0.2}As_2$ depends evidently on the Sr content, while the critical temperature T_c ranges from 17.3 to 21.7 K as measured in the resistivity data. Our structural analysis demonstrates that the lattice parameters a, c and the unit cell volume increased with the decrease of x in all of the $Ba_{1-x}Sr_xFe_2As_2$. Filtered TEM imaging reveals a visible inhomogeneous distribution of Ba/Sr elements in $Ba_{0.5}Sr_{0.5}Fe_2As_2$ which could result in relatively wider superconducting transitions in these layered materials.

Acknowledgments

This work is supported by the National Nature Science Foundation of China, the Knowledge Innovation Project of the Chinese Academy of Science and the 973 Project of the Ministry of Science and Technology of China.

References

[1] Kamihara Y, Watanabe T, Hirano M and Hosono H 2008 *J. Am. Chem. Soc.* **130** 3296
[2] Zhao J *et al* 2008 *Nat. Mater.* **7** 953
[3] Chen G F, Li Z, Wu D, Li G, Hu W Z, Dong J, Zheng P, Luo J L and Wang N L 2008 *Phys. Rev. Lett.* **100** 247002
[4] Chen X H, Wu T, Wu G, Liu R H, Chen H and Fang D F 2008 *Nature* **453** 761
[5] Ren Z A *et al* 2008 *Europhys. Lett.* **82** 57002
[6] Cheng P, Yang H, Jia Y, Fang L, Zhu X, Mu G and Wen H H 2008 *Phys. Rev.* B **78** 134508
[7] Ren Z A, Yang J, Lu W, Yi W, Che G C, Dong X L, Sun L L and Zhao Z X 2008 *Mater. Res. Innov.* **12** 105
[8] Millo O, Asulin I, Yuli O, Felner I, Ren Z A, Shen X L, Che G C and Zhao Z X 2008 *Phys. Rev.* B **78** 092505
[9] Li L J, Li Y K, Ren Z, Luo Y K, Lin X, He M, Tao Q, Zhu Z W, Cao G H and Xu Z A 2008 *Phys. Rev.* B **78** 132506
[10] Wang C *et al* 2008 *Europhys. Lett.* **83** 67006
[11] Ni N, Nandi S, Kreyssig A, Goldman A I, Mun E D, Bud'ko S L and Canfield P C 2008 *Phys. Rev.* B **78** 014523
[12] Ronning F, Klimczuk T, Bauer E D, Volz H and Thompson J D 2008 *J. Phys.: Condens. Matter* **20** 322201
[13] Chen G F, Li Z, Li G, Hu W Z, Dong J, Zhou J, Zhang X D, Zheng P, Wang N L and Luo J L 2008 *Chin. Phys. Lett.* **25** 3403
[14] Sasmal K, Lv B, Lorenz B, Guloy A M, Chen F, Xue Y Y and Chu C W 2008 *Phys. Rev. Lett.* **101** 107007
[15] Rotter M, Tegel M and Johrendt D 2008 *Phys. Rev. Lett.* **101** 107006
[16] Sefat A S, Jin R, McGuire M A, Sales B C, Singh D J and Mandrus D 2008 *Phys. Rev. Lett.* **101** 117004
[17] Jeevan H S, Hossain Z, Kasinathan D, Rosner H, Geibel C and Gegenwart P 2008 *Phys. Rev.* B **78** 092406
[18] Huang Q, Qiu Y, Bao W, Lynn J W, Green M A, Chen Y, Wu T, Wu G and Chen X H 2008 *Phys. Rev. Lett.* **101** 257003
[19] Torikachvili M S, Budko S L, Ni N and Canfield P C 2008 *Phys. Rev. Lett.* **101** 057006
[20] Wu G, Liu R H, Chen H, Yan Y J, Wu T, Xie Y L, Ying J J, Wang X F, Fang D F and Chen X H 2008 *Europhys. Lett.* **84** 27010
[21] Rotter M, Tegel M, Johrendt D, Schellenberg I, Hermes W and Pöttgen R 2008 *Phys. Rev.* B **78** 020503(R)
[22] Hu W Z, Dong J, Li G, Li Z, Zheng P, Chen G F, Luo J L and Wang N L 2008 *Phys. Rev. Lett.* **101** 257005
[23] Dong J *et al* 2008 *Europhys. Lett.* **83** 27006
[24] Leithe-Jasper A, Schnelle W, Geibel C and Rosner H 2008 *Phys. Rev. Lett.* **101** 207004
[25] Krellner C, Caroca-Canales N, Jesche A, Rosner H, Ormeci A and Geibel C 2008 *Phys. Rev.* B **78** 100504 (R)